Electronic Supplementary Material (ESI) for ChemComm.

A Co^{II} Complex for ^{19}F MRI Detection of Reactive Oxygen Species

Supporting Information

Meng Yu, Da Xie, Khanh P. Phan, José S. Enriquez, Jeffrey J. Luci, Emily L. Que

Materials and Methods	S2
Synthetic Methods	S5
Scheme S1. Synthesis of Co^{II}NODA-CF_3 (**2**)	S5
Figure S1. LC/MS traces of **2**	S8
Figure S2. Cyclic voltammogram of **2** in phosphate buffer	S10
Figure S3. IR spectra of Compound **1**, **2**	S10
Figure S4. Optimized structure of **2** obtained with DFT calculations	S11
Figure S5. UV/vis spectra of **2** in aerated buffer during 20 h	S11
Figure S6. ^{19}F NMR spectra of **2** reacting with O_2 and H_2O_2	S12
Figure S7. Determination of pseudo-first order rate constants of **2** reacting with H_2O_2	S13
Figure S8. Percentage of **2** oxidation at different pH conditions	S14
Figure S9. ^{19}F NMR spectra of **2** fully oxidized by H_2O_2	S14
Figure S10. Reduction of **3** by $Na_2S_2O_4$ in HEPES buffer	S15
Figure S11. ^{19}F NMR spectra of **3** and after reduction with excess $Na_2S_2O_4$	S15
Figure S12. Oxidation and reduction cycles of **2** by ^{19}F NMR	S16
Figure S13. ^{1}H NMR spectrum of **1** in D_2O	S17
Figure S14. ^{13}C NMR spectrum of **1** in D_2O	S18
Figure S15. ^{1}H NMR spectrum of **5** in $CDCl_3$	S19
Figure S16. ^{13}C NMR spectrum of **5** in $CDCl_3$	S20
Figure S17. ^{1}H NMR spectrum of **2** in D_2O	S21
Figure S18. ^{1}H NMR spectrum of **3** in D_2O	S22
References	S22

Materials and Methods

Materials

Except where stated otherwise, all chemicals were purchased from Sigma-Aldrich and Fisher Scientific and used as received. Deuterated solvents were purchased from Cambridge Isotope Laboratories. 1,4,7-Triazacyclononane (TACN) was synthesized through a published procedure.[1] 5-fluorocytosine was used as a standard for the ^{19}F NMR experiments.

Instrumentation

All ^{1}H, ^{13}C and ^{19}F NMR spectra were recorded on a 400 MHz Agilent NMR spectrometer; all reported resonances were referenced to internal standards. T_1 relaxation time was determined using the inversion-recovery method and T_2 relaxation time was measured using the CMPG pulse sequence. Walk-up LC/MS and high-resolution Electrospray Ionization (ESI) mass spectral analyses were performed by the Mass Spectrometry Facility of the Department of Chemistry at UT Austin. All cyclic voltammetry was performed under N_2 at 294 K using a CHI 660D electrochemical workstation at the UT Austin Center for Electrochemistry, a platinum working electrode, a platinum wire auxiliary electrode, and a Ag/AgCl (1M KCl) reference electrode. Inductively coupled plasma optical emission spectrometry (ICP-OES) was performed on a Varian 710 Series ICP-OES in EWRE lab in the Department of Civil, Architectural and Environmental Engineering at the University of Texas at Austin. Solid state infrared spectra were recorded on a Bruker Alpha spectrometer equipped with a diamond ATR crystal.

Determination of magnetic moment.

The effective magnetic moment was determined based on Evans' method.[2] A degassed solution of 10 or 15 mM **2** in D_2O, containing 5% tert-butanol by volume was placed in an NMR coaxial tube with 5% tert-butanol (v/v) in D_2O as reference. The effective magnetic moment (μ_{eff}) was calculated at 298 K (T) by using the equations given below. Δf stands for the proton chemical shift of *tert*-butanol in frequency (Hz) between the reference and paramagnetic sample, the spectrometer frequency (f) in Hz, the mass of the substance per mL of the solution (m), and the mass susceptibility of deuterium oxide (χ_0 = -0.6466 x 10^{-6} cm^3/g). The last term in eq. (2) is neglected. The molar susceptibility (χ_m) is the product of χ_g times the molecular weight of **2**. The experiment was repeated two times and averaged.

$$\chi_g = (-3\Delta f)/(4\pi fm) + \chi_0 + [\chi_0 (d_0-d_S)]/m \quad \textbf{eq. (1)}$$

$$\mu_{eff} = 2.84 (\chi_m T)^{1/2} \quad \textbf{eq. (2)}$$

DFT calculations

The structure of **2** was optimized using density functional theory (DFT) calculations without symmetry constraints.[3] The Becke's three–parameter hybrid exchange

functional with Lee-Yang-Parr gradient-corrected correlation (B3LYP functional[4]) was used with Lanl2dz pseudo-potential basis set[5,6] for Co and 6-31G(d,p) basis set for main group elements, as implemented in the Gaussian 09 package. Solvent correction (water) was considered and simulated using the polarizable continuum model (PCM).[7]

*Kinetic stability of **2***

5 mM of **2** was mixed with equivalent amount of Zn^{2+}, Ca^{2+} or Fe^{2+} in 50 mM degassed HEPES buffer (pH = 7.2) containing 0.1 M NaCl and incubated at 37 ºC under N_2. ^{19}F NMR spectra were taken periodically and compared with the control sample without any metal ions to determine the extent of transmetallation. After 24h, no measureable transmetallation was observed by NMR, suggesting that <5% of complex had dissociated over that period.

*Air stability of **2***

1.0 mM of **2** was dissolved in 50 mM aerated HEPES buffer (pH = 7.2) containing 0.1 M NaCl. The UV/vis absorbance was tracked overnight. ^{19}F NMR spectra were also taken to monitor the oxidation process. No noticeable change was observed after 20h based on NMR and UV/vis. Approximately 4% Co(II) complex was oxidized after 40h.

Kinetic Study of the H_2O_2 oxidation

The kinetic experiments were performed under pseudo first-order conditions with 0.76 mM of **2** and excess amount of H_2O_2 (7.0-15 mM). The reactions were conducted in 50 mM HEPES buffer (pH 7.4) containing 0.1 M NaCl under room temperature. The Co(III) complex has a distinct absorption feature at 518 nm while the Co(II) complex exhibits very weak absorbance around this region. Therefore the absorbance change at 518 nm was monitored over time. The pseudo first-order rate constants were determined by plotting $\ln(A/A_0)$ versus time ('A' represents the real time absorbance at 518 nm and 'A_0' stands for the initial absorbance at 0 min). Plotting of the pseudo first-order constants as a function of $[H_2O_2]$ gives a second-order rate constant of 0.12 $M^{-1}s^{-1}$. The first-order dependence on **2** was also confirmed by plotting the initial rate of oxidation (proportional to $\Delta A/\Delta t$: absorbance change rate at 518 nm) versus the concentration of Co(II) complex (0.6-1.2 mM).

pH dependence of H_2O_2 reaction

The effect of pH on the reaction rate was studied qualitatively by performing the reaction in HEPES buffer with pH values ranging from 6.8-8.0. The experiment was conducted with 2 mM Co^{II}NODA-CF_3 and 4 mM H_2O_2. The solution was stirred for 30 min and ^{19}F NMR was performed for individual samples using 5F-cytosine as the internal standard. The integrations of peaks were used to calculate the oxidation percentage.

Reduction of Co(III) complexes by sodium dithionite

To assess the reversibility of O_2 and H_2O_2 oxidation, the Co(III) complexes **3** and **4**

were reduced with excess of sodium dithionite in de-aerated HEPES buffer. The solution was kept in a cuvette sealed with a gas tight screw cap. The UV/Vis absorbance was monitored overnight and the pseudo first-order rates were determined. The ^{19}F NMR spectra were also acquired to confirm the full reduction of Co(III) complexes.

Selectivity towards other ROS

In order to evaluate the reactivity of **2** towards other reactive oxygen species (ROS), the Co(II) complex **2** was reacted with O_2^-, •OH, •O^{t}Bu, $ONOO^-$, *tert*-butyl hydroperoxide (TBHP) and ClO^-. The reactions were analyzed by NMR spectroscopy. O_2^- was generated by adding DMSO solution of KO_2 (catalytic amount of catalase was added to scavenge H_2O_2); •OH and •O^{t}Bu were made using Fenton chemistry by reacting $(NH_4)_2Fe(SO_4)_2$ or ^{t}BuOOH with H_2O_2; $ONOO^-$ was generated in situ by mixing $NaNO_2$ with H_2O_2; TBHP was introduced by adding 70% TBHP in water; ClO^- was generated through adding aqueous solution of NaClO.[8,9] Solutions were analyzed 30 minutes after reagents were combined. The experiments were done in 50 mM HEPES buffer (pH 7.4) with 2 mM **2** and 2 eq. of ClO^-, TBHP, KO_2, $ONOO^-$, •OH and •O^{t}Bu.

Cyclic voltammetry

Electrochemistry experiments were carried out on a CHI 660D electrochemical workstation. A three-electrode cell was used, including a platinum electrode as working electrode, an Ag/AgCl (1 M KCl) aqueous electrode as reference electrode and a platinum wire as auxiliary electrode. The solutions were degassed with N_2 before measurements.

^{19}F MRI Experiments

The magnetic resonance imaging experiments were performed on a Bruker BioSpin (Karlsruhe, Germany) Pharmascan 70/16 magnet with a BioSpec two-channel console and BGA-9s gradient coil. The RF coil was a quadrature single resonance tunable T/R coil (Doty Scientific, Inc., Columbia, South Carolina, USA) with a resonant frequency of 282.2 MHz to correspond to ^{19}F at 7.0 T. Each element of the RF coil was tuned and matched with the samples loaded using a Morris frequency sweeper (Morris Instruments, Inc. Ottawa, Ontario, Canada) while the complementary element was terminated with the receive chain of the instrument. All prescan adjustments and imaging was performed using product sequences and methods in ParaVision 6.0.1 (Bruker, vide supra). Solutions were imaged while contained in standard 200 μL Eppendorf tubes mounted in a 3×3 grid by a custom holder produced on a Form 2 3D printer (FormLabs, Inc., Somerville, Massachusetts, USA). Images were spin-density weighted using a Rapid Acquisition with Relaxation Enhancement (RARE, aka Fast Spin-Echo or FSE) sequence with a TR/effTE/ES/ETL of 700ms/3.68ms/3.68ms/4 at 50 kHz receive bandwidth and tailored RF pulses. The geometry of the imaging was

defined by a single slice 25mm thick in a horizontal plane, a field-of-view of 35×35 mm^2, and covered by a 64×64 acquisition matrix. Images were acquired in 50 min. Using these parameters, any signal between -70 and -80 ppm will be observed, with sharper peaks appearing brighter.

Synthetic Methods

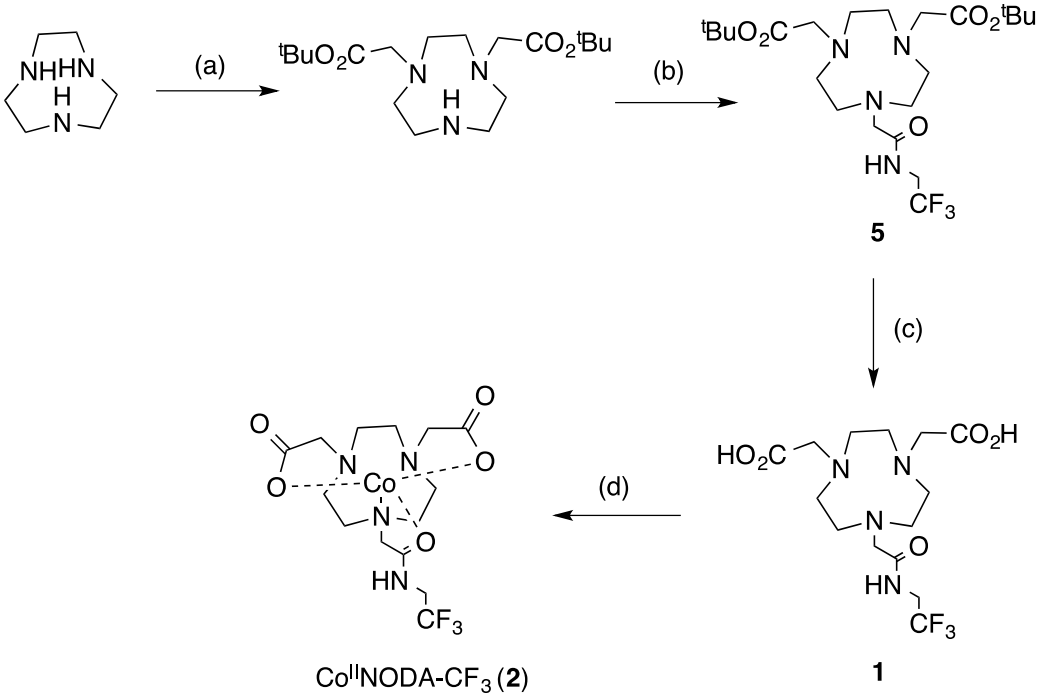

Scheme S1. Synthesis of Co^{II}NODA-CF_3 (**2**). Conditions: (a) *tert*-butyl bromoacetate, $CHCl_3$(anhy.), r.t., 24 h (32%); (b) 2-chloro-*N*-(2,2,2-trifluoroethyl)acetamide, KI, K_2CO_3, MeCN(anhy.), 65 ºC, 16 h (90%); (c) TFA/TIS/H_2O (95/2.5/2.5, v/v/v), 0 ºC-r.t., 16 h (75%); (d) $CoCl_2$•$6H_2O$, pH~6-7, 3 h (70%)

2-chloro-*N*-(2,2,2-trifluoroethyl)acetamide

NaOH (0.608 g, 15.2 mmol) was dissolved in 5 mL deionized water. 2,2,2-trifluoroethylamine hydrochloride (1.0 g, 7.38 mmol) in 6 mL water was added followed by 8.5 mL *t*-BuOMe, and the mixture was stirred for 30 min at 0-5 ºC. Chloroacetyl chloride (0.878 g, 7.77 mmol) in 1.5 mL *t*-BuOMe was slowly added to the solution and stirred for 1 h while maintaining the temperature at 5-10 ºC. The solution was warmed up to r.t. and extracted with *t*-BuOMe. The organic fractions were combined and dried over Na_2SO_4. Evaporation of solvent yielded 850 mg of white crystalline powder, which was used without further purification. ^{1}H NMR (400 MHz, $CDCl_3$, 25 ºC): δ 6.89 (bs, -NH, 1H), 4.13 (s, 2H), 3.97 (m, 2H). ^{13}C NMR (100 MHz, $CDCl_3$, 25 ºC): δ 166.54, 125.26, 122.49, 42.51, 41.31, 40.96. ^{19}F NMR (376 MHz, $CDCl_3$, 25 ºC): δ -72.45 (t, *J* = 8.9 Hz).

1,4-Bis(tert-butoxycarbonylmethyl)-1,4,7-triazacyclononane

1,4,7-Triazacyclononane (TACN) (1.08 g, 8.36 mmol) was dissolved in 20 mL dry $CHCl_3$ and cooled on an ice bath. *tert*-Butyl bromoacetate (3.58 g, 18.4 mmol) in 40 mL dry $CHCl_3$ was added over two hours using an addition funnel. The mixture was stirred under r.t. for a further 24 h and the solvent was removed to produce a yellow oil. The crude product was purified using C18 reverse phase chromatography to yield 1.1 g of product as a hydroscopic powder in 32% yield (eluant A: MeCN (contain 0.1% formic acid), eluant B: H_2O (contain 0.1% formic acid); the column was equilibrated at 100% B for 2 min, then ramped to 30% A over 8 min, the product was obtained at 30% A). ^{1}H NMR (400 MHz, $CDCl_3$, 25 ºC): δ 3.34 (s, 4H), 3.11 (t, 4H), 3.00 (t, 4H), 2.74 (s, 4H), 1.43 (s, 18H). ^{13}C NMR (100 MHz, $CDCl_3$, 25 ºC): δ 170.88, 82.03, 56.66, 51.41, 48.63,44.09, 28,30. LRMS (ESI$^+$): Calcd for MH^+ ($C_{18}H_{36}N_3O_4$) 358.3, found 358.3.

4,7-Bis(tert-butoxycarbonylmethyl)-1,4,7-triazacyclononane-1-*N*-(2,2,2-trifluoroethy-l)acetamide (5)

1,4-Bis(tert-butoxycarbonylmethyl)-1,4,7-triazacyclononane (486 mg, 1.36 mmol), 2-chloro-*N*-(2,2,2-trifluoroethyl)acetamide (243 mg, 1.38 mmol), KI (450 mg, 2.72 mmol), and anhydrous K_2CO_3 (563 mg, 4.08 mmol) were mixed in 25 mL anhydrous MeCN and stirred at 65 ºC under N_2 for 16 h. The solution was cooled to r.t., filtered, and the solvent was removed to yield a viscous yellow oil. The crude product was purified by C18 reverse phase to yield 600 mg product as a pale yellow powder in 90% yield (eluant A: MeCN (contain 0.1% formic acid), eluant B: H_2O (contain 0.1% formic acid); the column was equilibrated at 100% B for 2 min, then ramped to 30% A over 10 min, the product was obtained at 30% A). ^{1}H NMR (400 MHz, $CDCl_3$, 25 ºC): δ 3.91 (m, 2H), 3.48 (t, 2H), 3.33 (s, 4H), 2.90 (m, 8H), 2.77 (m, 4H), 1.44 (s, 18H). ^{13}C NMR (100 MHz, $CDCl_3$, 25 ºC): δ 170.86, 81.62, 60.52, 58.68, 56.05, 55.13, 53.74, 40.83, 40.49, 28.32. ^{19}F NMR (376 MHz, $CDCl_3$, 25 ºC): δ -71.99 (t, J = 9.4 Hz). LRMS (ESI$^+$): Calcd for MH^+ ($C_{22}H_{40}F_3N_4O_5$) 497.3, found 497.3.

4,7-Bis(carboxymethyl)-1,4,7-triazacyclononane-1-*N*-(2,2,2-trifluoroethy-l)acetamide (1)

Compound **5** (600 mg, 1.21 mmol) was dissolved in trifluoroacetic acid (10 mL), triisopropylsilane (260 µL) and deionized water (260 µL) at 0 °C. The solution was warmed to r.t. and stirred for 16 h. The solvent was removed and coevaporated with dichloromethane multiple times. The residual TFA was further removed by reverse phase chromatography to afford 397 mg product as a white hydroscopic powder (75% yield). (eluant A: MeCN (contain 0.1% formic acid), eluant B: H_2O (contain 0.1% formic acid); the column was equilibrated at 100% B for 5 min, then ramped to 25% A over 10 min, the product was obtained at 25% A). ^{1}H NMR (400 MHz, D_2O, 25 ºC): δ 3.95 (m, 2H), 3.77 (s, 4H), 3.59 (s, 2H), 3.28 (s, 4H), 3.16 (m, 4H), 2.90 (m, 4H). ^{13}C NMR (100 MHz, D_2O, 25 ºC): δ 174.30, 172.69, 59.03, 56.72, 50.82, 49.11, 48.34, 40.37, 40.02.

^{19}F NMR (376 MHz, D_2O, 25 ºC): δ -71.86 (dt, *J* = 4.0, 9.4 Hz). HRMS (ESI$^+$): Calcd for MH^+ ($C_{14}H_{24}F_3N_4O_5$) 385.1693, found 385.1695.

Co^{II}NODA-CF_3 (2)

Compound **1** (100 mg, 0.263 mmol) was dissolved in 1 mL de-aerated milli-Q water and the pH was adjusted to approximately 7 with 1 M NaOH solution. Then $CoCl_2$•$6H_2O$ (64 mg, 0.269 mmol) in 1 mL de-aerated water was slowly added and the pH was adjusted back to 7. The solution was stirred under N_2 for 3 h and lyophilized. The crude was purified by reverse phase chromatography (70% yield). (eluant A: MeCN (contain 5% ammonium acetate solution), eluant B: 50 mM ammonium acetate solution (pH 6.5, solution was purged with N_2 before using); the column was equilibrated at 100% A for 5 min and then eluted with 100% B for 5 min before loading the sample, the product was obtained at 4 min using B as eluant. ^{19}F NMR (376 MHz, D_2O, 25 ºC): δ -75.6 (s, br). HRMS (ESI$^+$): Calcd for MH^+ ($C_{14}H_{22}CoF_3N_4O_5$) 442.0869, found 442.0883.

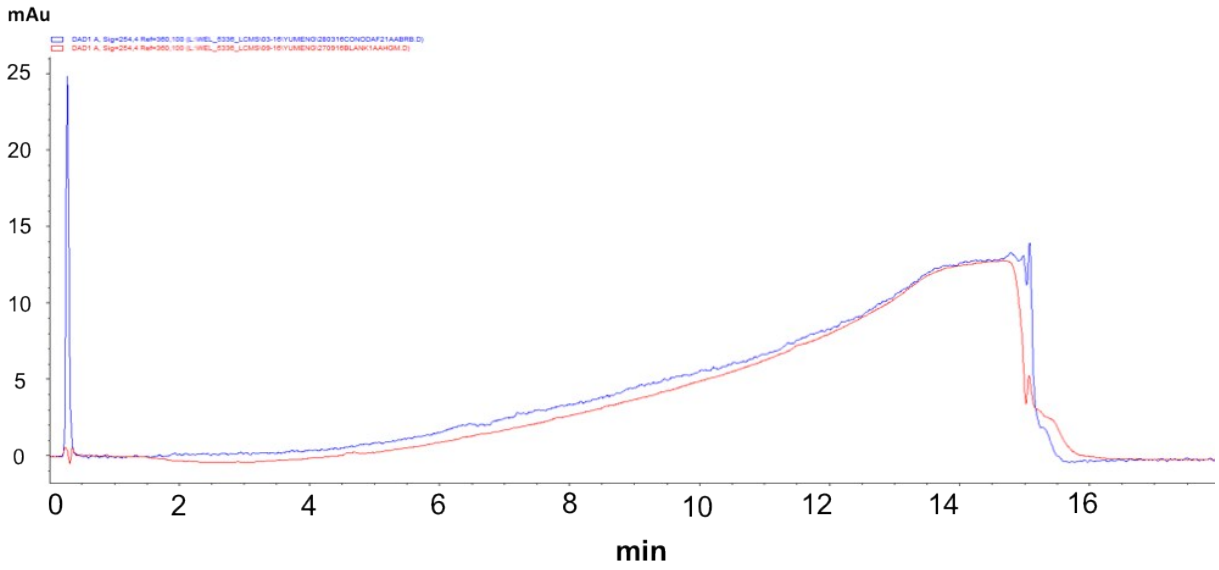
mAu
25
20
15
10
5
0
0
2
4
6
8
10
12
14
16
min

(a)

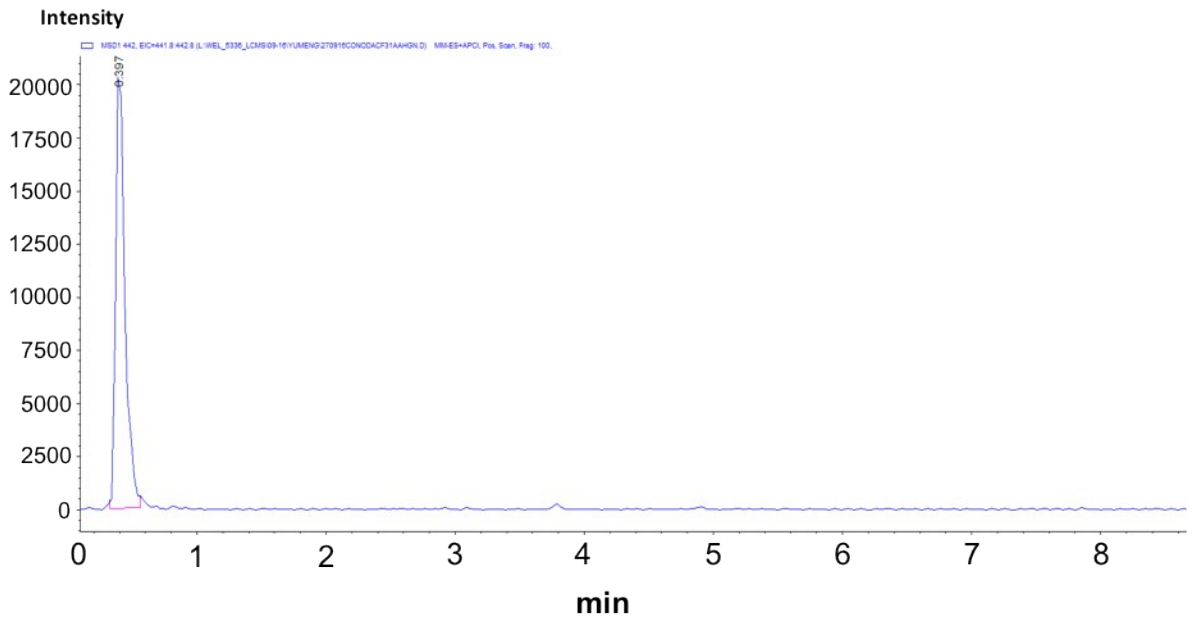
Intensity
20000
17500
15000
12500
10000
7500
5000
2500
0
0
1
2
3
4
5
6
7
8
min

(b)

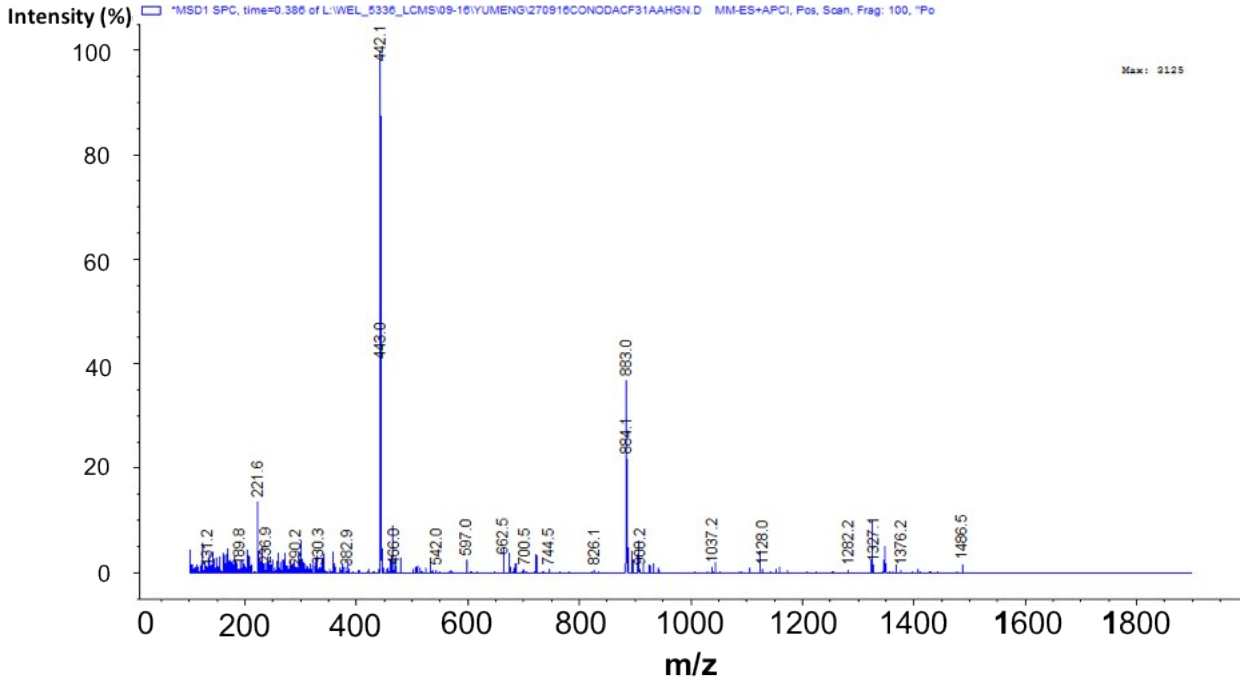

(c)

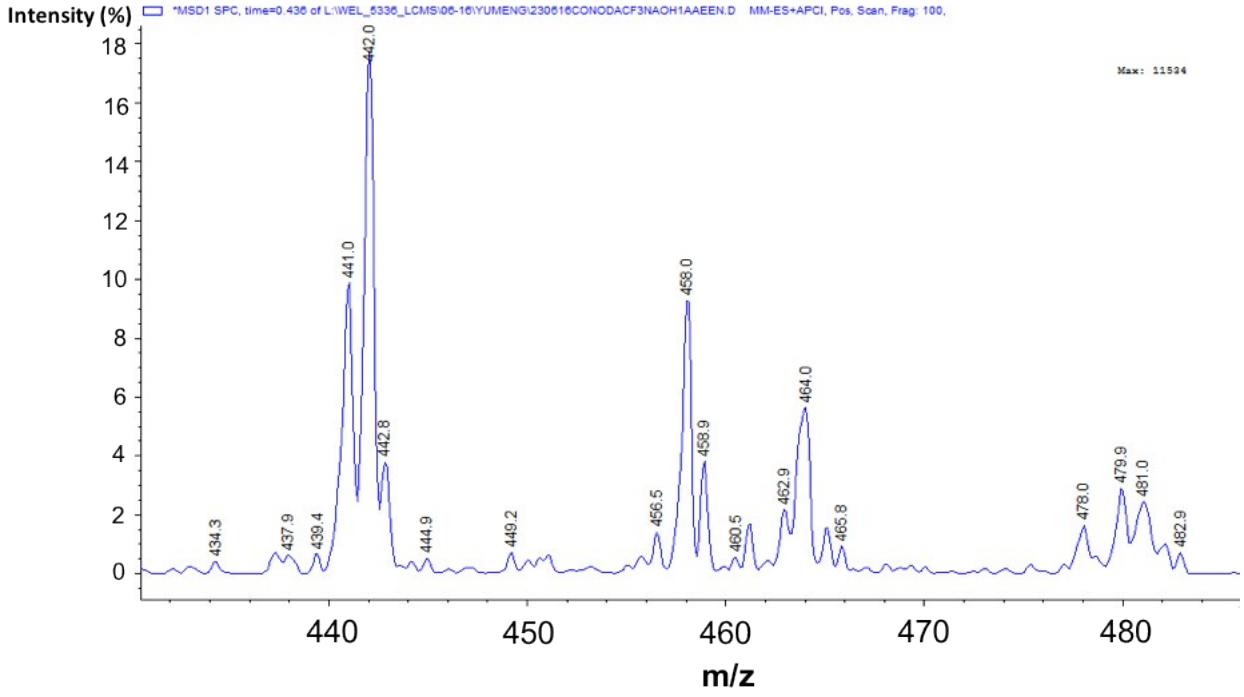

(d)

Figure S1. (a) LC/MS UV trace overlay of **2** (blue) and blank (red) (254 nm, Gemini C18 3.5 micron 2.1 x 50 mm, 0.7 mL/min, 5-95% MeCN/H_2O (0.1% FA) in 12 min); (b) LC/MS mass spectrum trace of **2** (positive mode ESI/APCI); (c) Mass spectrum of

LC/MS trace (positive mode). The peak at 442.1 corresponds to $[M+H]^+$, 883.0 corresponds to $[2M+H]^+$; (d) Mass spectrum of 2 mM **2** after reacting with 2 eq. H_2O_2 for 30 min. The peak at 441.0 corresponds to oxidized product **3** and the peaks at 458.0, 479.9 correspond to $[M+OH]^+$ and $[M+Na+O]^+$.

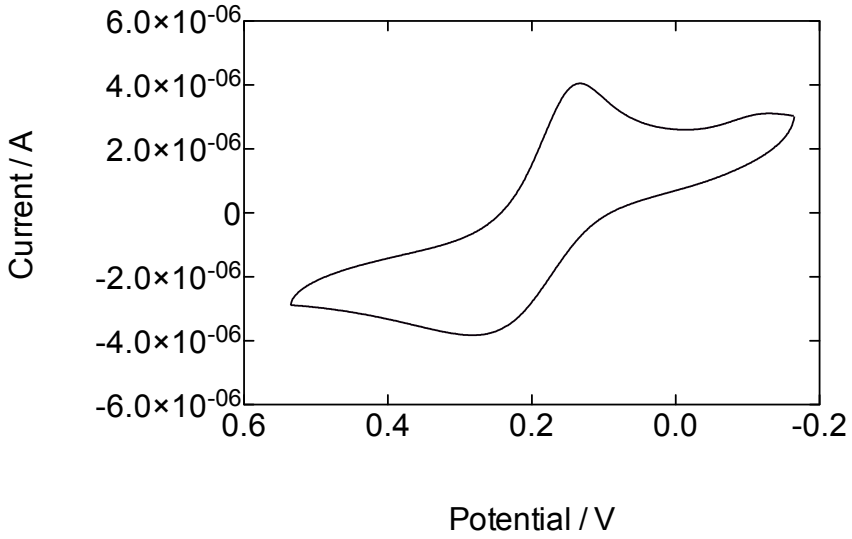

Figure S2. Cyclic voltammogram of 1.0 mM **2** in 0.1 M Na_2HPO_4/NaH_2PO_4 buffer, pH 7.2. Scan rate: 50 mV/s. Potentials are referenced vs. NHE.

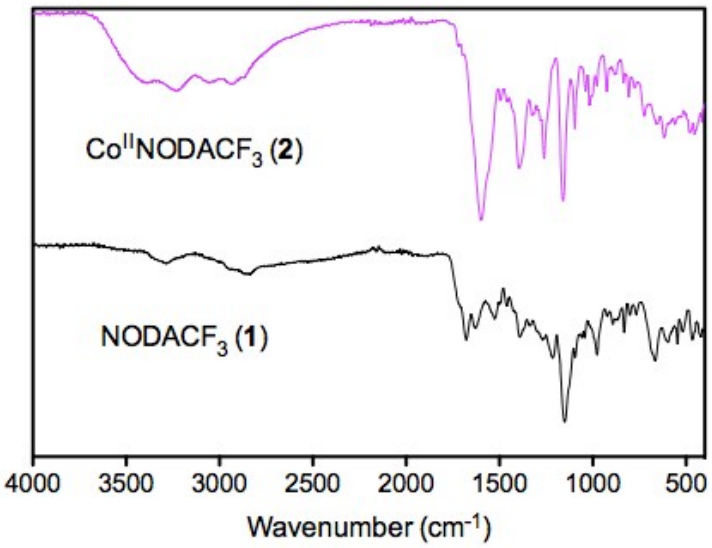

Figure S3. IR spectra of solid NODA-CF_3 **1**, Co^{II}NODA-CF_3 **2**.

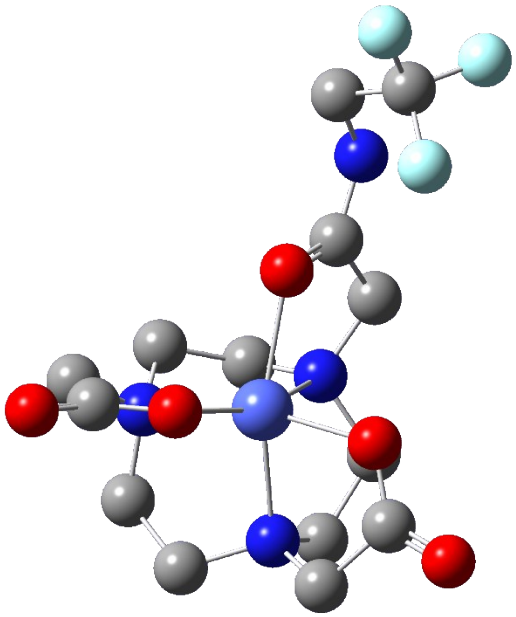

Figure S4. Optimized structure of Co^{II}NODA-CF_3 (**2**) obtained with DFT calculations. The hydrogen atoms were removed for clarity.

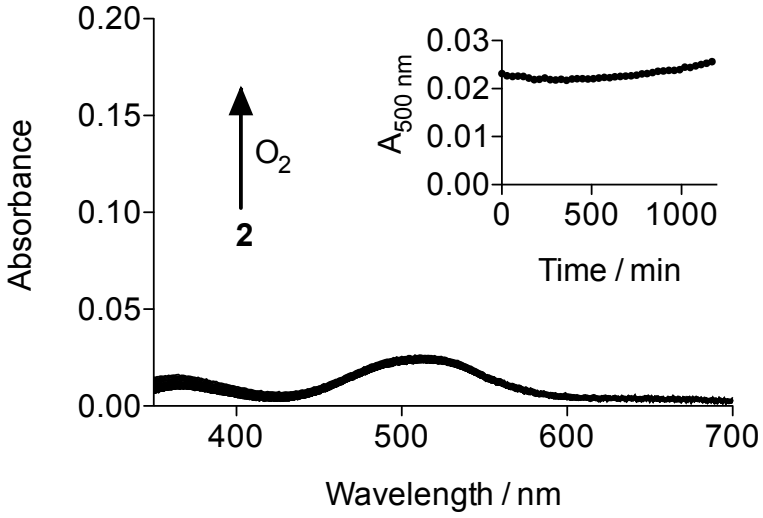

Figure S5. UV/vis spectra of 1.0 mM **2** in 50 mM HEPES buffer (pH 7.2) during 20 h (inset: absorbance change at 500 nm over time).

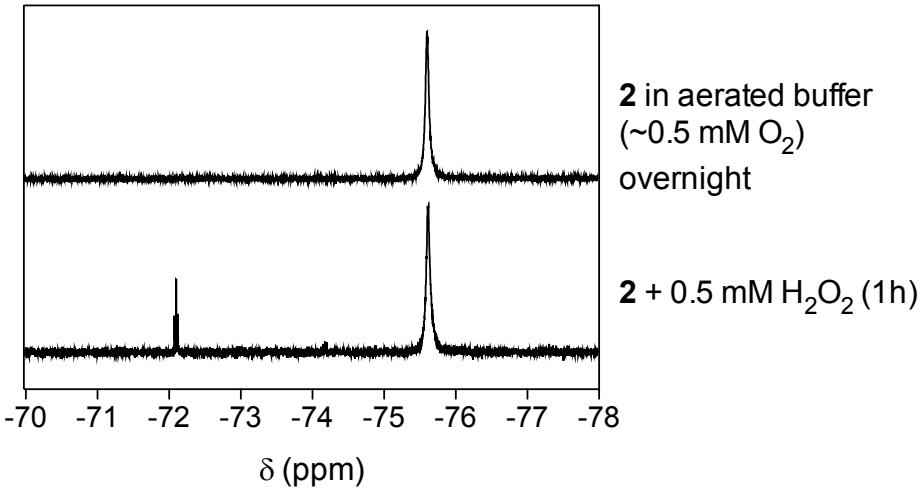

Figure S6. ^{19}F NMR spectra of 2 mM Co(II) complexes **2** after incubating in aerated buffer overnight ([O_2] ~0.5 mM) and after reacting with 0.5 mM H_2O_2 for 30 min. The peak at 75.6 ppm corresponds **2**; the peak at 72.2 ppm corresponds to **3**.

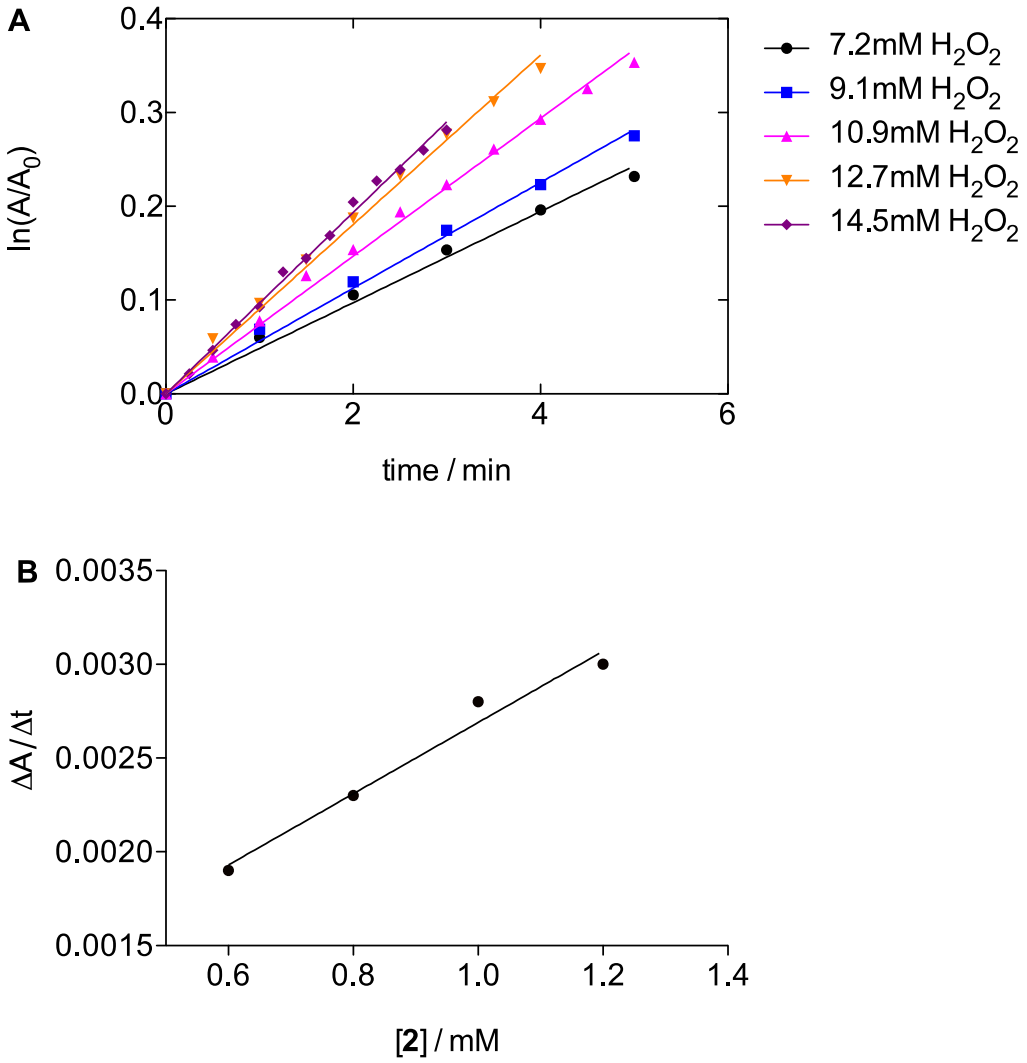

Figure S7. (A) Plot of $\ln(A/A_0)$ versus time. Slope of the linear curve fit gives pseudo first-order rate constant k_{obs}. (B) Plot of initial absorbance change rate at 518 nm versus [**2**]. The linear relationship indicates the first-order dependence on **2**.

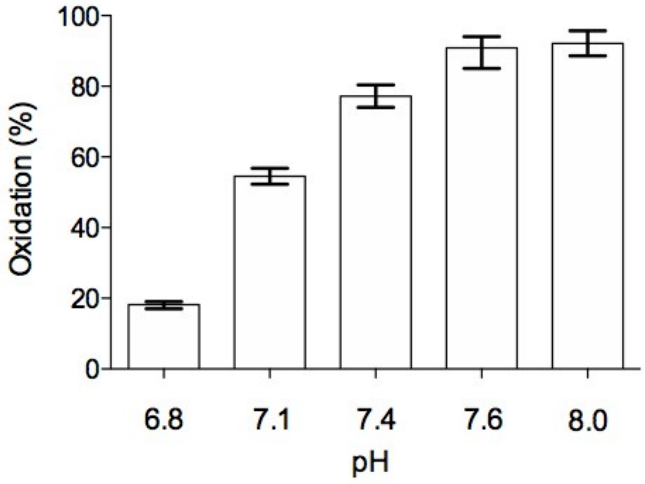

.

Figure S8. Percentage of **2** oxidation by H_2O_2 in buffers of different pH determined by ^{19}F NMR using 5F-cytosine as the internal standard. The integrations of peaks were used to calculate the oxidation percentage. The experiments were performed in 50 mM HEPES buffer containing 0.1 M NaCl under room temperature. 2 mM **2** and 4 mM H_2O_2 were used and reacted for 30 min.

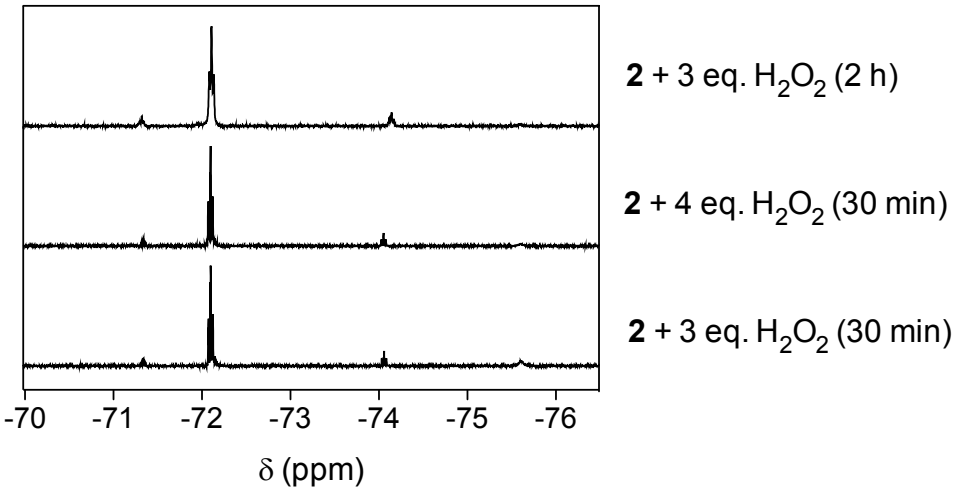

Figure S9. ^{19}F NMR spectra of 2 mM Co(II) complexes **2** after reacting with 3 equiv. H_2O_2 for 30 min, 2 h and 4 equiv. H_2O_2 for 30 min. The peak at 75.6 ppm corresponds to residual **2**; the peak at 72.2 ppm corresponds **3**; the peaks at -71.3 and -74.1 ppm correspond to side oxidation products with ligand being oxidized as indicated in Figure S1(d).

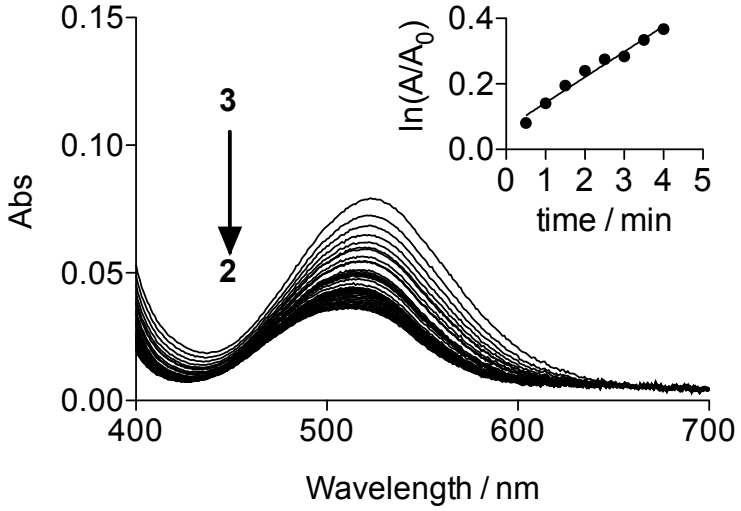

Figure S10. Reduction of 0.38 mM **3** by 10 mM $Na_2S_2O_4$ in degassed HEPES buffer (pH 7.2); **3** was generated *in situ* by reacting **2** with three equivalents of H_2O_2 for an hour Inset: determination of pseudo first-order rate constant by plotting $\ln(A_0/A)$ versus time.

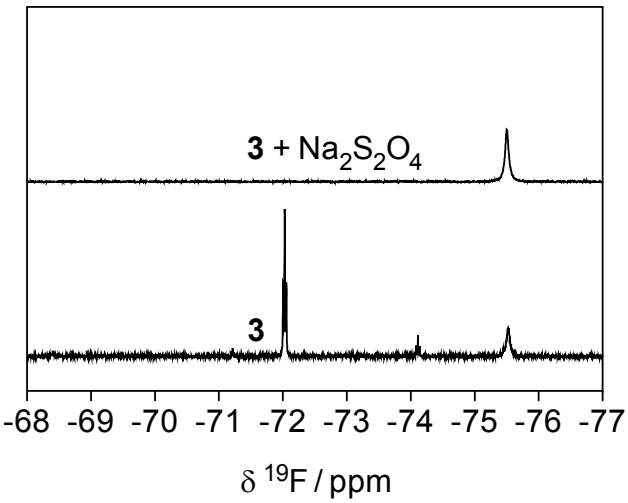

Figure S11. ^{19}F NMR spectra of Co(III) complexes **3** and after reduction with excess $Na_2S_2O_4$. The peak at 75.6 ppm corresponds to **2**; the peak at 72.0 ppm corresponds to **3**; the peaks at -71.2, and -74.1 ppm correspond to side oxidation products with ligand being oxidized as indicated in Figure S1(d).

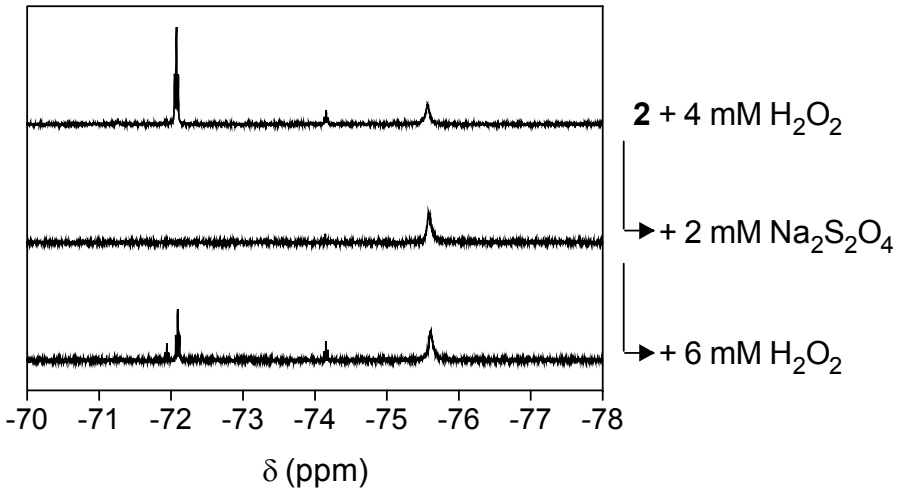

Figure S12. ^{19}F NMR spectra of 2 mM **2** after reacting with 4 mM H_2O_2 for 30 min, after reduction with 2 mM $Na_2S_2O_4$ overnight and after reacting with 6 mM H_2O_2 for 1 h. The peak at 75.6 ppm corresponds to **2**; the peak at 72.2 ppm corresponds to **3**; the peaks at -71.3, and -74.1 ppm correspond to side oxidation products with ligand being oxidized as indicated in Figure S1(d); the peak at -71.9 ppm could be assigned to free ligand.

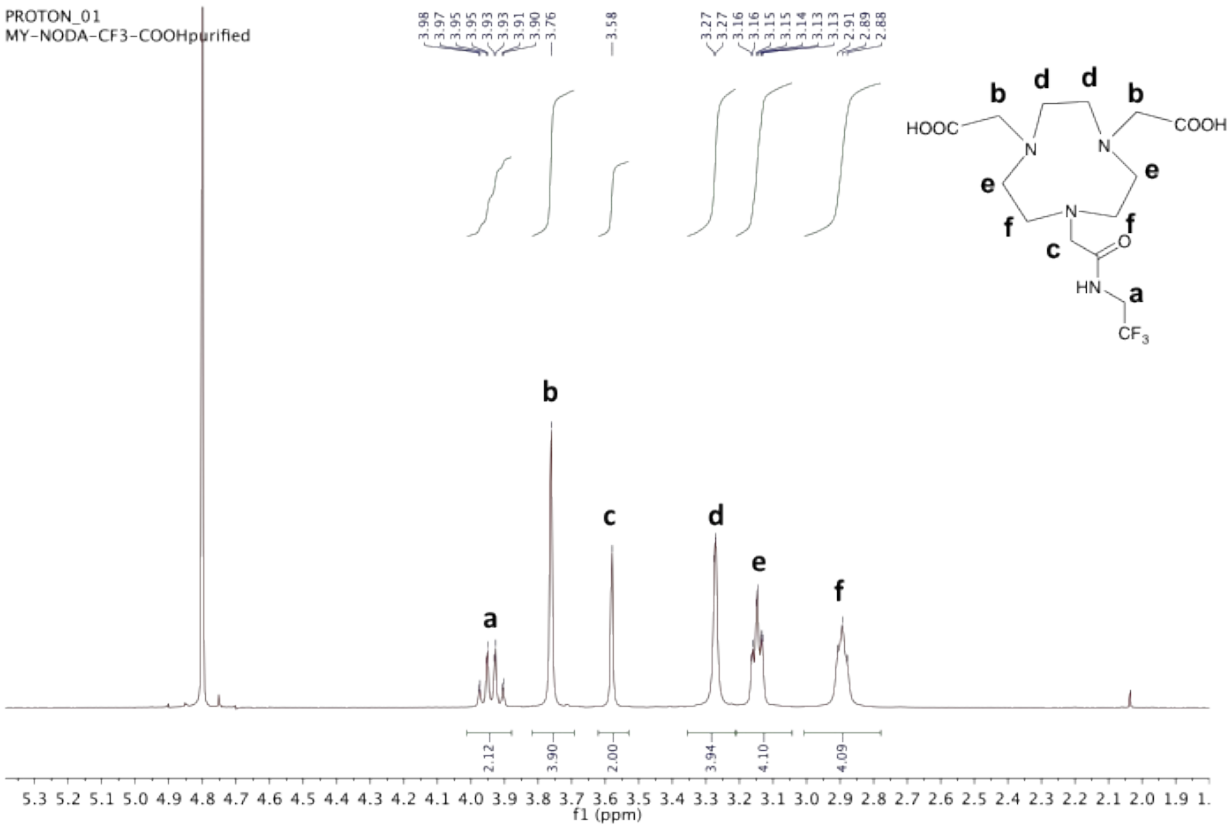

Figure S13. ^{1}H NMR spectrum of NODA-CF_3 (**1**) in D_2O.

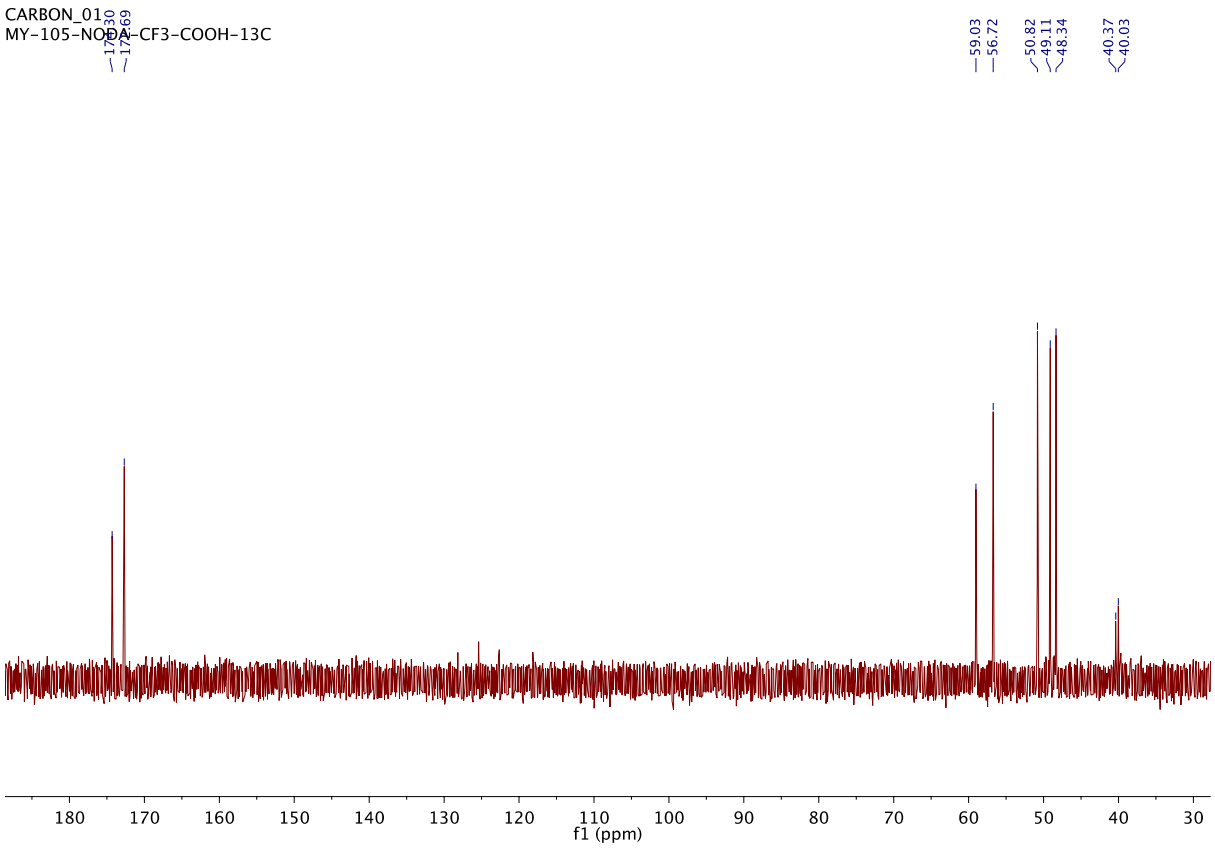

Figure S14. ^{13}C NMR spectrum of NODA-CF_3 (**1**) in D_2O.

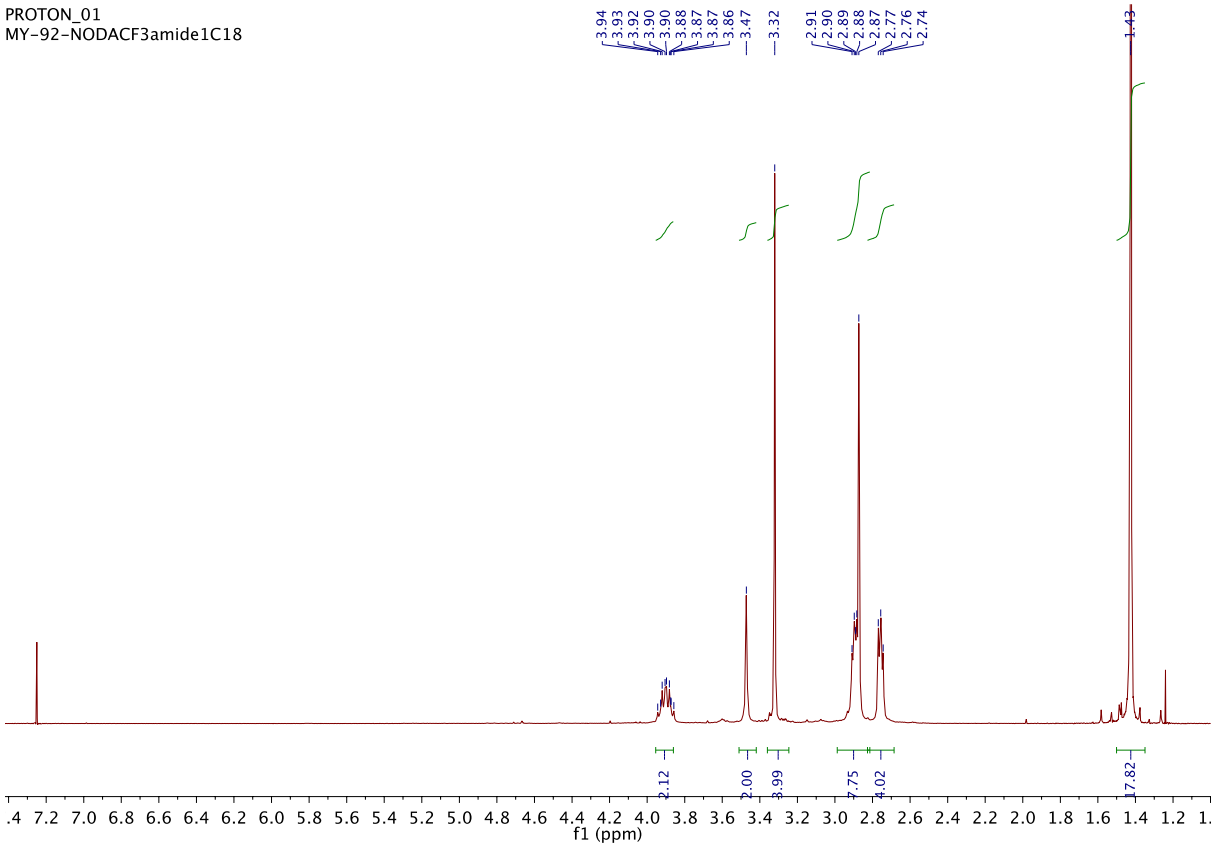

Figure S15. ^{1}H NMR spectrum of **5** in $CDCl_3$.

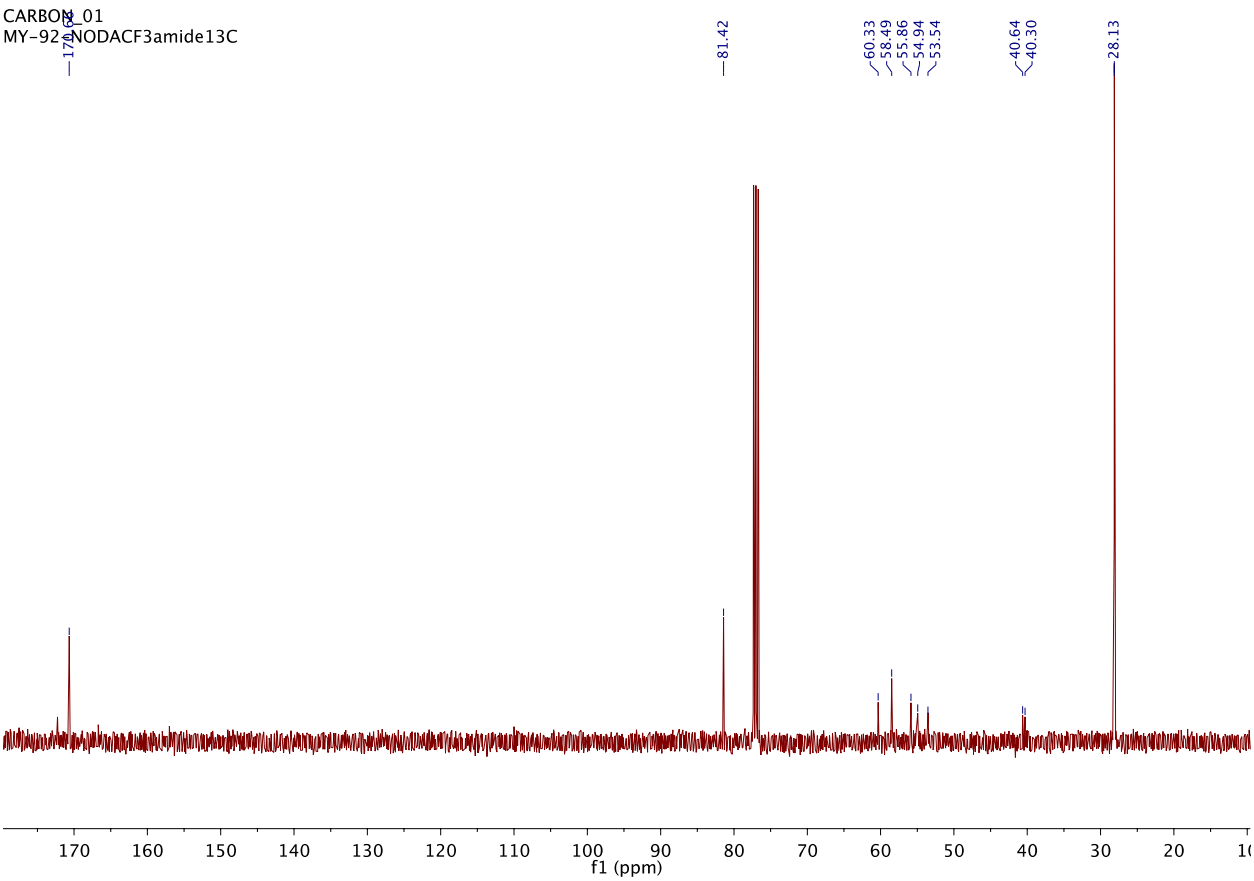

Figure S16. ^{13}C NMR spectrum of **5** in $CDCl_3$.

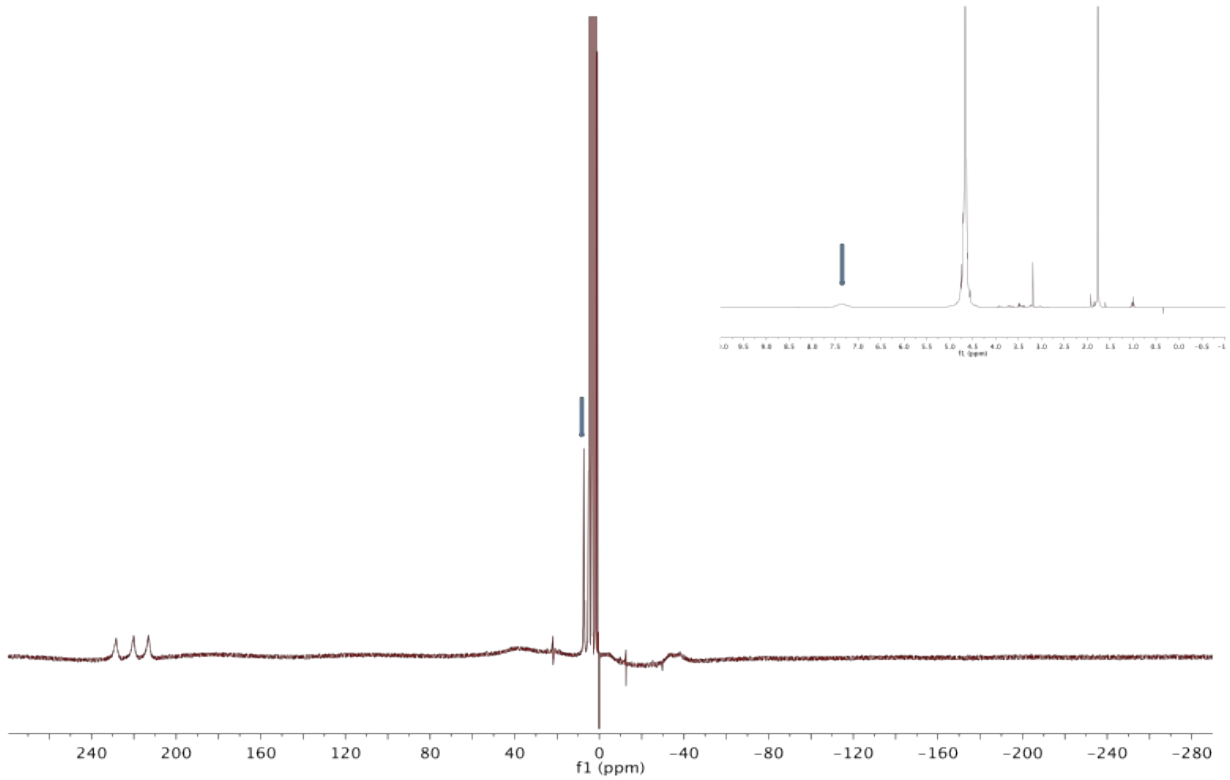

Figure S17. ^{1}H NMR spectrum of 10 mM **2** in D_2O. Arrow in inset indicates a broad peak at ~7.5 ppm.

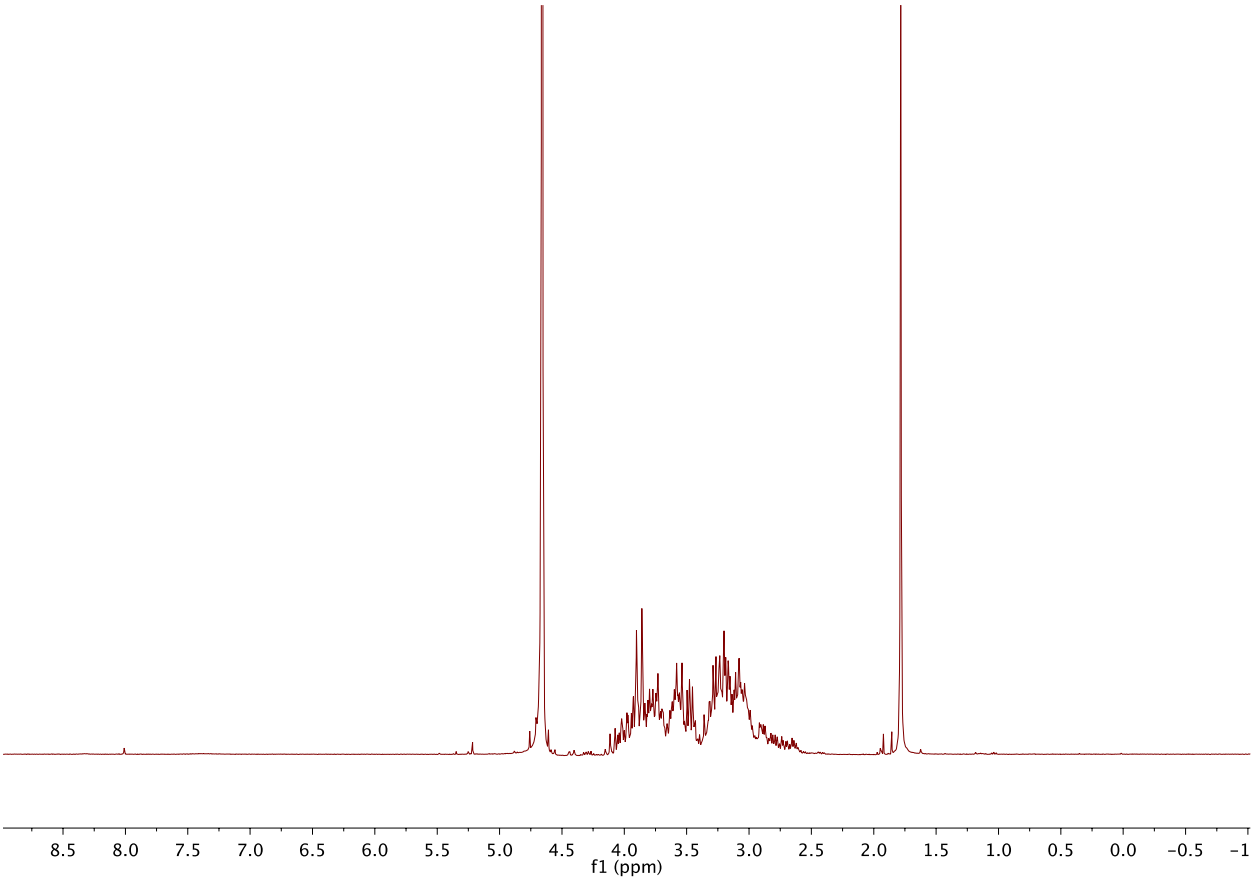

Figure S18. ^{1}H NMR spectrum of 10 mM **3** in D_2O.

References

[1] K. V. Tan, P. A. Pellegrini, B. W. Skelton, C. F. Hogan, I. Greguric, P. J. Barnard, *Inorg. Chem.* **2014**, *53*, 468–477.

[2] D. F. Evans, *J. Chem. Soc.* **1959**, 2003.

[3] A. D. Laurent, D. Jacquemin, *Int. J. Quantum Chem.* **2013**, *113*, 2019–2039.

[4] A. D. Becke, *J. Chem. Phys.* **1993**, *98*, 5648.

[5] P. J. Hay, W. R. Wadt, *J. Chem. Phys.* **1985**, *82*, 270–283.

[6] P. J. Hay, W. R. Wadt, *J. Chem. Phys.* **1985**, *82*, 299–310.

[7] G. Scalmani, M. J. Frisch, *J. Chem. Phys.* **2010**, *132*, 114110.

[8] Zhang, R.; Zhao, J.; Han, G.; Liu, Z.; Liu, C.; Zhang, C.; Liu, B.; Jiang, C.; Liu, R.; Zhao, T.; Han, M.-Y.; Zhang, Z. *J. Am. Chem. Soc.* **2016**, *138*, 3769.

[9] Lippert, A. R.; Keshari, K. R.; Kurhanewicz, J.; Chang, C. J. *J. Am. Chem. Soc.* **2011**, *133*, 3776.